Tuning and controlling the shape of mesoporous silica particles with CTAB/sodium deoxycholate catanionic mixtures

Leana Travaglini,[a*] Pierre Picchetti,[a] Alessandra Del Giudice,[b] Luciano Galantini,[b] Luisa De Cola [a,c*]

[a] Université de Strasbourg, CNRS, ISIS UMR 7006, 8 allée Gaspard Monge, 67000 Strasbourg, France.

[b] Dipartimento di Chimica, Sapienza Università di Roma, P.le A. Moro 5, 00185 Rome, Italy

[c] Institut für Nanotechnologie (INT) - Building 640, Karlsruhe Institute of Technology (KIT) - Campus Nord, Hermann-von-Helmholtz-Platz 1, 76344 Eggenstein-Leopoldshafen, Germany.

E-mail: travaglini@unistra.fr, decola@unistra.fr

Fax: + 33 (0)3 68 85 52 42; Tel. +33 (0)3 68 85 52 20

Abstract

Controlling the shape and size of mesoporous silica particles (MSPs) requires a deep understanding of the different parameters that play a major role during the synthesis of the materials. One of the key factors that can determine the morphology and porosity of the systems is the surfactant, used as a templating agent. We have very recently proven that binary mixtures of hexadecyltrimethylammonium bromide (CTAB) and bile salts are templating systems effective in controlling the morphology of MSPs in a facile and non-costly way. In this work we investigated the effect of different surfactant ratios in order to gain deeper insights on the influence of these catanionic mixtures on particle morphology. We employed mixtures of CTAB and sodium deoxycholate (NaDC) and upon variation of a sole parameter, the NaDC concentration, we achieved shape tuning. Hexagonal platelets, rods, oblate and toroidal particles were obtained and fully characterized. Moreover, investigation of the CTAB/NaDC assemblies showed that the morphology tuning is related to the evolution of the mixed micelles properties, occurring upon variation of the surfactant ratio.

Keywords: morphology tuning, mesoporous silica particles, bile salts, catanionic mixtures

1. Introduction

Mesoporous silica particles (MSPs) have attracted considerable attention due to their potential in numerous applications, which include catalysis, sensing, separation techniques

and drug delivery.[1-3] Their versatility lies in the ease of functionalization due to silica chemistry and in the controllable surfactant-templated process, which allow for tailoring the MSPs properties according to the desired application.[4-7] Much effort has been devoted to prepare materials with different mesostructure, size, porosity and network composition, leading to particles with tunable features and desired properties.[4-11] In designing ideal materials, the particle overall morphology is a crucial aspect to be taken into account. The extent to which molecules access pores or, when it comes to bio-related applications, particles interact with cells highly depends on the particle shape and aspect ratio.[12-15] Nevertheless, a fine control and tuning of MSPs shape is still a major challenge in the field and simple methodologies to achieve the desired morphology are a desirable goal. When the syntheses are performed in diluted conditions,[16, 17] the MSPs morphology results from the competition between free surface energy and mesostructure formation free energy.[18] The shape can be therefore influenced by all those parameters inducing variations on the interactions between the micelles and the growing silicates and/or on silicates hydrolysis and condensation rates.[18-20] Dilution, pH value, temperature, salt additives, catalyst, type and concentration of both surfactants and co-solvents are all responsible for the final shape. Moreover, the morphology tuning in basic conditions remains particularly challenging since the formation of MSPs with lowest surface energy, say spherical particles, is favored due to the high silica condensation rate.[21]

In order to have controllable and tunable morphologies, different synthetic strategies have been reported in the literature, generally requiring the variation of several parameters. In both acid [19, 22-25] and basic media,[20, 26-31] the effect of concentration, solvent, temperature, (co)-surfactants, organic and inorganic additives or type of co-solvents was investigated and plentiful morphologies have been so far described.[3, 5, 32, 33] Particles with different shapes were also obtained upon introduction of specific organoalkoxysilicates, enabling the control of morphology of organo-doped and periodic mesoporous silica particles.[34-39] Such an extensive investigation certainly clarified the effect of various single parameters on the synthesis of MSPs but, to the best of our knowledge, the preparation of various morphologies upon variation of a single parameter by using a facile and cost-effective *bottom up* method has yet to be addressed.

In this context, we have recently disclosed the potential of mixtures composed of CTAB and bile salts in controlling the morphology of MCM-41 particles in alkaline aqueous media at 25 and 50 °C.[40] The method allowed us to prepare submicrometer MSPs with various

shapes and high porosity, in particular well-separated hexagonal platelets and twisted rods with chiral pores channels and tunable aspect ratio. We showed that the specific interactions between CTAB and the bile salts are responsible for the morphology variation and, in the same experimental conditions, different bile salts (namely lithocholate, deoxycholate and cholate) have different effects. Their influence on the particle shape can be related to the different hydrophilic/hydrophobic balance, given by the number of -OH groups borne on the steroidal moiety. Bile salts are non-conventional facial amphiphiles characterized by a unique aggregation behavior [41-45] and they associate with CTAB forming complex mixed micelles. The bile salt molecules insert into the micelle core to avoid contact with water while the carboxylate groups strongly interact with the cationic head group of CTAB. The interaction between the two surfactants and the properties of the resulting aggregates depend not only on the type of BS but also on the ratio between the oppositely charged surfactants.[46-55]

Herein we report a detailed investigation on the effect of CTAB/bile salt catanionic mixtures when employed at different ratios. In particular, we employ sodium deoxycholate (NaDC, Fig. 1) due to its intermediate hydrophobicity but also to the fact that its interaction with CTAB has been widely investigated.[46-51] NaDC was introduced in the system at various concentrations to explore the effect of different binary mixture compositions on the material final morphology. We intended to exploit the properties of the mixed micelles at different CTAB/NaDC ratios to induce variations in the growth of mesoporous silica particles. Following the recently reported synthetic protocol[40] and keeping constant the concentration of CTAB, the amount of NaDC was increased gradually to assess the effect of different compositions of the binary mixtures on the shape of the mesoporous silica material.

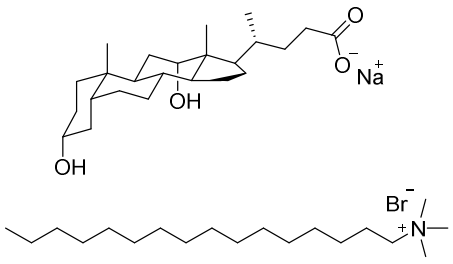

Fig. 1 Molecular structure of sodium deoxycholate (NaDC, top) and the hexadecyltrimethylammonium bromide (CTAB, bottom) used as surfactants.

This strategy successfully permits us to modulate the morphology of submicrometer MSPs in alkaline conditions upon variation of only one parameter, the NaDC concentration. Spheres, rugby ball-like particles, hexagonal platelets, rods, fibers, toroids, have been prepared and thoroughly characterized to assess both their morphology and porosity by means of scanning and transmission electron microscopy (SEM and TEM), small-angle X-ray scattering (SAXS) and nitrogen physisorption measurements. In addition, dynamic light scattering (DLS), electrophoretic mobility (μ) and synchrotron-SAXS measurements have been performed on CTAB/NaDC mixtures at the utilized ratios in order to unravel the interactions between the two surfactants and correlate them with the different observed particles growths.

2. Experimental Section

2.1 Materials

All reagents and solvents were used as obtained. Hexadecyltrimethylammonium bromide (CTAB, 99+%) was purchased from ACROS ORGANICS. Sodium deoxycholate (NaDC, ≥ 97%), tetraethyl orthosilicate (TEOS, ≥ 99.0 %, GC) and all solvents were purchased from Sigma Aldrich. Aqueous ammonia (NH_3, 28 wt.%) was purchased from VWR Chemicals.

2.2 Preparation of particles

The particles were prepared by following the protocol we have recently described.[40] CTAB and NaDC were used as structure directing agents. The reactions were performed by keeping constant the amount of CTAB, while the amount of NaDC was varied between 2.5 and 90 in weight percentage vs CTAB. In a typical synthesis, H_2O (25 mL) was added to CTAB (50 mg, 0.14 mmol) and NaDC, the mixture was stirred and gently heated up until complete dissolution was observed and then it was allowed to cool down to 25 °C and stirred for 10 min. Aq. NH_3 28 wt.% (1.42 mL, 22.90 mmol) was added and the mixture stirred at 750 rpm for further15 min. MeOH (0.10 mL, 3.95 mmol) and TEOS (0.25 mL, 1.28 mmol) were then added and the mixture stirred for 90 min. The mixture was left under static conditions for further 20 h. The solid material was recovered by centrifugation and the precipitate washed with distilled H_2O (x3) and EtOH (x2). The particles were purified by

means of ultracentrifugation and the surfactants removed through calcination at 530 °C for 6 h, unless otherwise stated.

2.3 Characterization.

Scanning electron microscopy (SEM) images were recorded with a FEI Quanta FEG 250 instrument (FEI corporate, Hillsboro, Oregon, USA) with acceleration voltage of 20 kV and operation distance of 10 mm. The samples were prepared by drop-casting a dispersion of particles in EtOH onto a glass cover slip, subsequently sputter coated with Au (Emitech K575X Peltier cooled) for 55 s at 60 mA prior to fixation on Al support.

Transmission electron microscopy (TEM) samples were analyzed on a FEI/PHILIPS CM120 system operating at 120 kV. Samples were prepared drop casting dispersions of particles in EtOH (0.1 mg/mL) onto Formvar-coated Cu grids (400 mesh) and allowed to dry overnight prior visualization.

N_2 physisorption isotherms of dried samples were obtained with a Micromeritics ASAP-2020 physisorption instrument. The samples were degassed at 250 °C for 6h and N_2 adsorption/desorption measurements were performed at -196 °C. The surface areas were calculated by Brunauer-Emmett-Teller (BET) method in the relative pressure P/P_0 range 0.06-0.3.[56] The pore size distributions and pore volumes were calculated by a DFT method on the adsorption branch. The adsorption data were analyzed using the SAIEUS software (model used: N_2@77K, cylindrical pores in an oxide surface)[57], provided by Micrometrics. The total pore volumes were estimated at P/P_0= 0.99.

The small-angle X-ray scattering (SAXS) set-up comprised the SAXSess mc^2 instrument from Anton Paar GmbH, containing a slit collimation system, and the PW3830 laboratory X-ray generator (40 kV, 50 mA) with a long-fine focus sealed X-ray tube (CuKα wavelength of λ = 0.1542 nm) from PANalytical. Detection was performed with the 2D imaging-plate reader Cyclone® by Perkin Elmer. Measurements were performed on powder samples for 5 min and the data collected up to a scattering vector q value of 7 nm^{-1}, where $q = (4\pi\sin\theta)/\lambda$ and 2θ the scattering angle. The 2D data were converted to 1D data by using SAXSQuant software (Anton Paar GmbH, Austria). The formula $d = 2\pi/q$ was used to calculate the d spacing. The average pore diameter has been determined using the equation for unit cell parameter $a_0 = (2/\sqrt{3})d_{100}$, which gives the pore center-to-center distance and subtracting 1.0 nm, an approximated value for the MCM-41 wall thickness.[58] The data on the CTAB/NaDC mixed aggregates were collected at the SWING beamline at the SOLEIL

synchrotron source (Saint-Aubin, France). SAXS patterns were recorded using a two-dimensional Eiger detector placed in a vacuum detection tunnel. The beamline energy was set at 12 keV and the sample-to-detector distance was around 3 m to cover the q range 0.0042-0.36 $Å^{-1}$. The Automated Injection Robot was employed to flow the samples (40 µl) in the quartz capillary (diameter 1.5 mm) for subsequent 490 ms exposures. Milli-Q water was used for subtraction. The software FoxTrot available at the beamline was employed for data reduction (circular integration, absolute intensity scaling based on water), for the selection of the most superimposable frames to be averaged and for background subtraction.

DLS and electrophoretic mobility (μ) measurements were performed with a Malvern Nano-ZetaSizer, equipped with a 5 mW HeNe laser (λ = 632.8 nm) and a digital logarithmic correlator. The normalized intensity autocorrelation functions were measured at an angle of 173° at 25.0 ± 0.1 °C. Dust was eliminated by means of a filtration through filters with a pore size of 0.22 mm. The data were analyzed by using the non-negative least square (NNLS) method which provided mono-modal volume distributions of the diameters. The peaks of these distributions were considered as representative of the apparent hydrodynamic diameter D_h of the micelles. The normalized average intensity I/c was also analyzed, where I is the average scattered intensity and c the total surfactant concentration (mass/volume). The normalization was performed in order to correct for the concentration of the scatterers and to extract the effect of their mass on the scattered intensity. As we worked at low electrolyte concentration, repulsive interactions between the micelles as well as counterion cloud fluctuations could affect the DLS data. These effects were neglected in the qualitative analysis reported in this work.

3. Results and discussion

The materials were prepared following the modified Stöber process that we recently reported.[40] The reaction was performed at 25 °C, using a CTAB/NaDC catanionic mixtures as templating system, an aqueous NH_3 solution as a catalyst, MeOH as a co-solvent and tetraethyl orthosilicate (TEOS) as the silica source (see section 2.1 for synthetic details). For the different material synthesis, the amount of CTAB was maintained fixed, while the amount of NaDC was varied between 2.5 and 90 in weight percentage vs CTAB (see Table 1). In our previous work,[40] we showed that in the identical employed experimental conditions the use of only CTAB as the structure directing agent led to particles characterized by spherical

geometry (average diameter of ca. 250 nm), 3.0 nm pores, and highly ordered hexagonal mesostructure, which is reflected by the presence of facets.

We found that the different amount of NaDC, as co-surfactant, has a dramatic effect on the shape of the mesoporous materials as clearly evidenced by the scanning electron microscopy (SEM, Fig. 2) analysis of the obtained materials. Already upon addition of 2.5 wt.% NaDC (sample 1, Fig. 2a) particles are no longer spherical but oblate and characterized by width of 360 ± 56 nm and height ranging from 220 to 280 nm (Fig. S1). Similarly, in sample 2 oblate particles were observed, showing though a slightly larger width of 408 ± 55 nm and height ranging from 210 to 270 nm (Fig. S2). These results suggest that the addition of NaDC leads to larger and flatter particles and this trend is confirmed by sample 3, as platelets with a hexagonal geometry were imaged (Fig. 2c). The platelets are characterized by mean width of 498 ± 56 nm and height ranging from 190 to 270 nm (Fig. S3), and do not show intergrowth or twinned aggregation. It is worth noting that this result is in agreement with our previous observations, since comparable hexagonal platelets were also obtained when the reaction was performed in the presence of an equimolar amount of deoxycholic acid.[40] This also shows that the same effect on the morphology is observed when the sodium salt is used and, at the same time, confirms that the effect on the growth of the particles is mainly due to the interactions between the two counter-charged surfactants, which induce a variation in the charge density and, subsequently, in the interactions with the growing silicates. The SEM micrographs showed the occurrence of elongated structures upon further increase of the ratio NaDC/CTAB. Short rods were present in sample 4 (Fig. 2d), while a variety of different structures was observed in sample 5, in particular C-, S-, U-shaped and twisted rods, gyroids and particles with seashell-like geometry (Fig. 2e). Sample 6 was composed of mainly short curved rods and, to a lesser extent, of toroidal particles while in sample 7 the toroidal structures are the predominant morphologies and only few short curved rods were present (Fig. 2f,g). Spherical objects up to 10-15 μm and amorphous particulate material were instead present in samples 8 and 9, prepared with 70 and 90 wt.% of NaDC (Fig. 2h, 2j, S4 and S5). It is interesting to note that in a typical synthesis, while for all samples after centrifugation and extraction ca. 35 mg of materials were recovered, from samples 8 and 9 only ca. 20 mg of silica were obtained. Moreover, all the materials were calcined at 530 °C for 6 h in order to remove the organic templates, without changing their morphologies, with the exception of the curved rods and toroidal particles (samples 6 and 7) that at this temperature showed

collapsing of their structure (Fig. S6). Therefore, for samples 6 and 7, the templates were extracted in hot HCl/EtOH, and the structures of the materials were preserved.

TEM analysis (Fig. 3) confirmed the morphology evolution and allowed investigating the mesostructure of the particles. In the oblate, plate- and rod-like particles of samples 1-4, pore channels running along the main symmetry axis (the shortest for oblates and platelets and the longest for rods) could be clearly observed (Fig. 3a, 3d and S7, S9). In sample 5, characterized by particles of different overall morphologies, the pore orientation varied depending on the particle shape. In the case of rods and curved twisted structures the pores run along the particle length, while for seashell-like particles concentric channels were imaged (Fig. 3e and S9). Micrographs recorded on samples 6 and 7 showed curved rods and toroids, respectively, confirmed the loss of ordering, and the channels seemed to run along the long dimension (Fig. 3f, 3g and S10). Ordered arrays of pore structures could not be imaged for samples 8 and 9 even on the smaller particles present (Fig. 3h and 3j).

Table 1 List of samples prepared by employing the different NaDC quantities and related morphological properties. The CTAB amount was 50 mg and it was maintained fixed in all reactions.

Sample	NaDC amount (mg)	NaDC amount (wt.%)	Shape	Size distribution* (nm)	Height range (nm)
1	1.25	2.5	oblate	360 ± 56	220-280
2	2.50	5	oblate	408 ± 55	210-270
3	5.00	10	hexagonal platelet	498 ± 85	190-270
4	7.50	15	hexagonal platelets + short rods	plat 450-600 rods 250-300	140-200 100-150
5	15.00	30	heterogeneous	250-600	-
6	20.00	40	curved rods	180-400	75-200
7	25.00	50	toroids + rods	tor 150-300 rod 300-700	90-140 60-80
8	35.00	70	spheres + amorphous	300-700	-
9	45.00	90	spheres + amorphous	200-12000	-

*****The mean value was calculated from the Gaussian size distribution obtained from SEM micrographs, counts on 100 particles. A range is given for heterogeneous samples. A range is given when from the EM micrographs is not possible to accurately measure the height value for a statistically relevant number of objects.

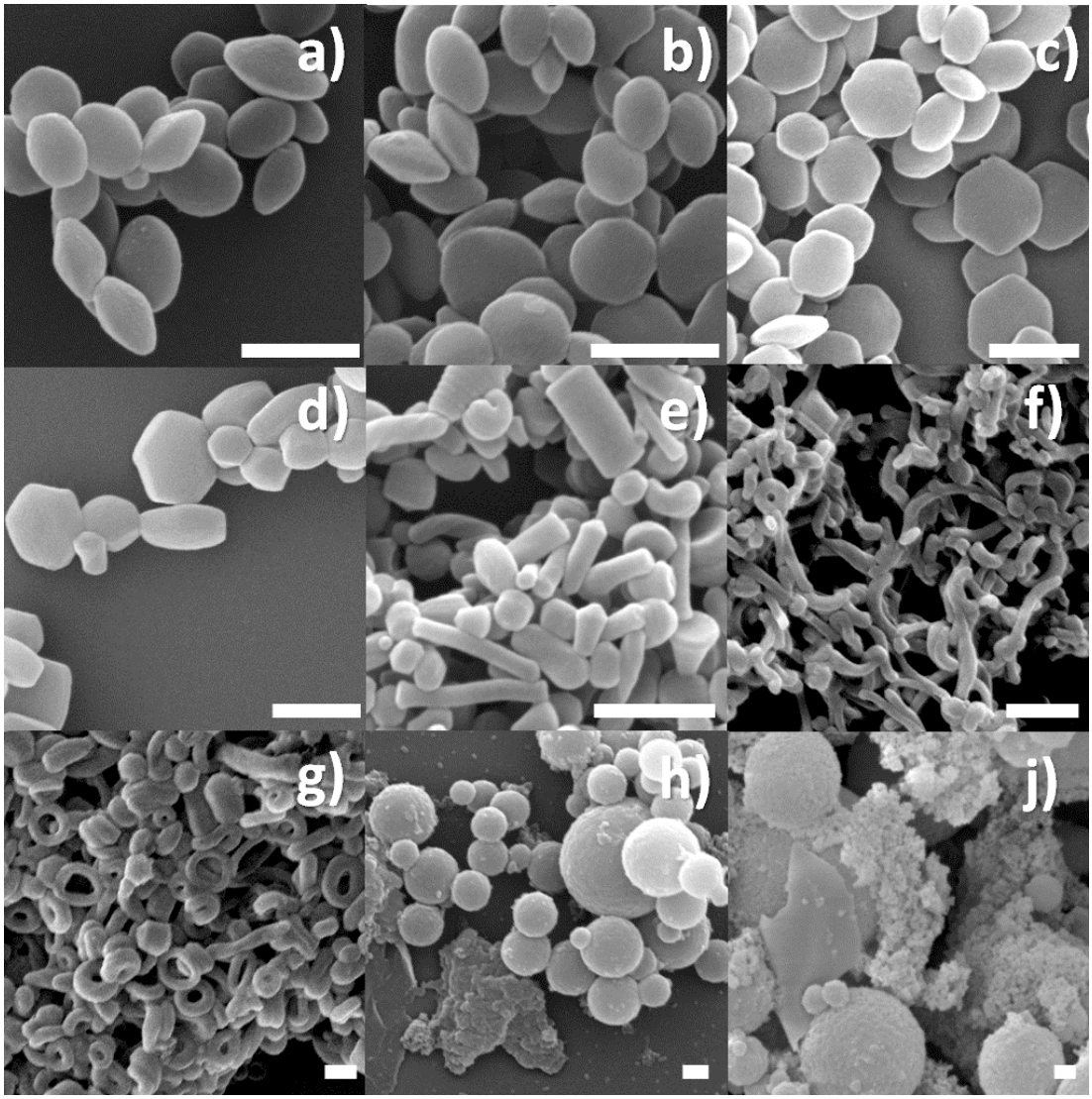

Fig. 2 SEM images of a) sample 1, b) sample 2, c) sample 3, d) sample 4, e) sample 5, f) sample 6, g) sample 7, h) sample 8 and j) sample 9. Scale bar = 500 nm.

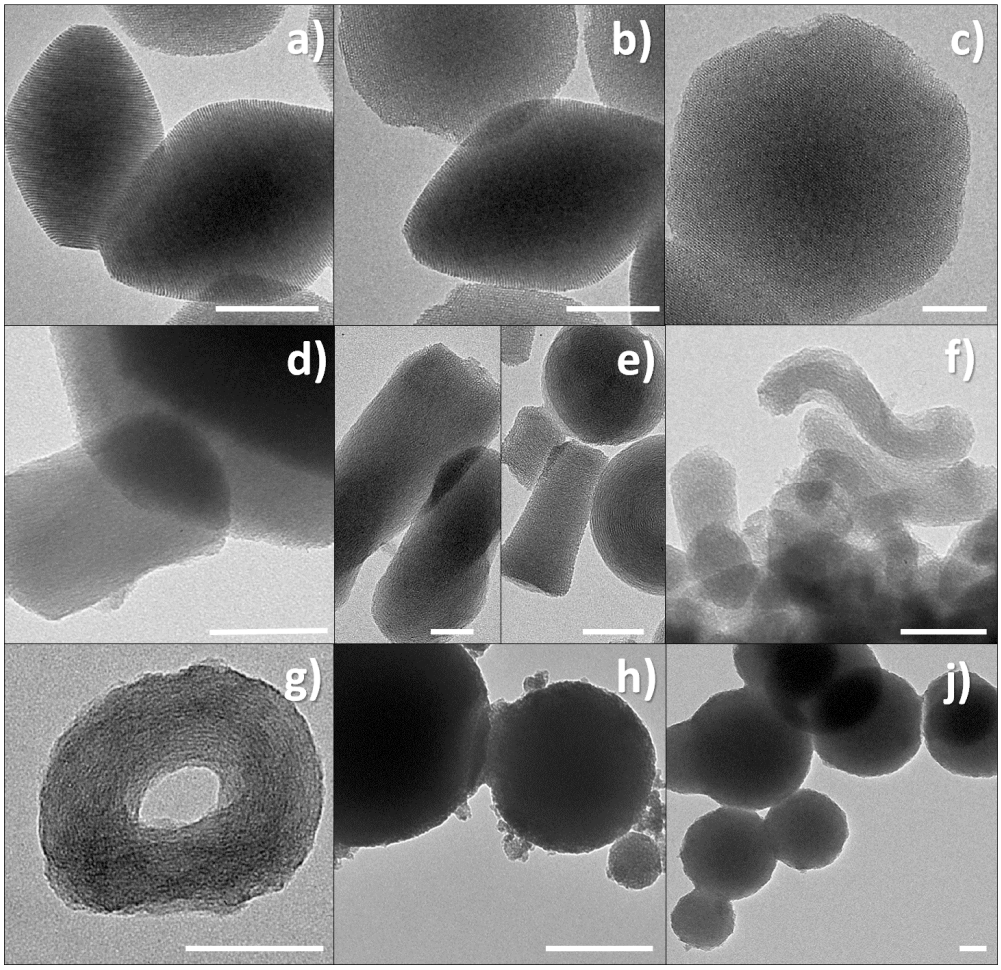

Fig. 3 TEM images of a) sample 1, b) sample 2, c) sample 3, d) sample 4, e) sample 5, f) sample 6, g) sample 7, h) sample 8 and j) sample 9. Scale bar = 100 nm.

SAXS analysis on the materials, after surfactants removal, was performed to investigate further the mesostructure. Fig. 4 revealed for sample 1 (NaDC 2.5 wt.%) the presence of three Bragg peaks at q = 1.88, 3.25 and 3.72 nm^{-1} that were indexed as the (100), (110) and (200) planes of MCM-41 materials, therefore related to a regular 2D hexagonal array of pores with *p*6*mm* symmetry. The distance between two pore centres in MCM-41 was calculated from the equation $a_0 = (2/\sqrt{3})d_{100}$, where a_0 is the unit cell parameter, and the pore diameter could be estimated subtracting 1.0 nm, an approximated value for the wall thickness,[57] thus resulting equal to 2.8 nm. Upon progressive increase of NaDC content, the (110) and (200) Bragg peaks were no longer visible and the (100) signal gradually becomes broader and less intense, hence suggesting the loss of long-range order, which was already significant at 30 wt.% of NaDC (sample 5).

The porosity of the particles was assessed by means of N_2 adsorption/desorption measurements (Fig. 5). Type IV isotherms, typical for mesoporous materials, were obtained for samples 1 to 6. The values of BET surface, total pore volume and average pore width obtained from data analysis are listed in Table 2 and showed the variation of porosity properties upon increase of NaDC wt.%. In fact, the pore diameter gradually decreased down to 2.6 nm in the hexagonal plate-like particles (sample 3). At the same time, a decrease of the total pore volume was also observed, from 0.61 (sample 1) to 0.51 cm^3/g (sample 3), explainable with the fact that the pore channels became shorter. A decrease of pore diameter was observed also for samples 4-6, however within these samples an increase of the total pore volume was observed in the case of samples 4 and 6 ones, most likely due to an increase of the channel packing density. Further, samples 4-5 showed a sort of double distribution of pores, explainable by the presence of both hexagonal platelets and rods having a different pore arrangement. For samples 5 and 6 the isotherms were slightly flatter at low relative pressure values, and this could be explained by the coexistence of micropores, although to a minimal extent. Sample 7 showed instead low BET specific surface area and total pore volume values, and this was highly likely due to the fact that pores, as suggested by TEM analysis, run along the closed toroidal structure and were therefore not accessible. The observed N_2 adsorption may be therefore related to the short-curved rods present in the sample (Fig. 2g and S10). Also, the width distribution suggested the presence of micropores, whose presence on the particles surface cannot be dismissed. The isotherms measured on samples 8 and 9 showed instead a large hysteresis probably due to interstitial voids between the small particulate material visible in the SEM images (Fig. 2h and 2j), reflected also in the pore width distributions at values >5nm. The contribution of the interstitial voids could also explain the increase of total average pore, which is calculated at $P/P_0 = 0.99$.

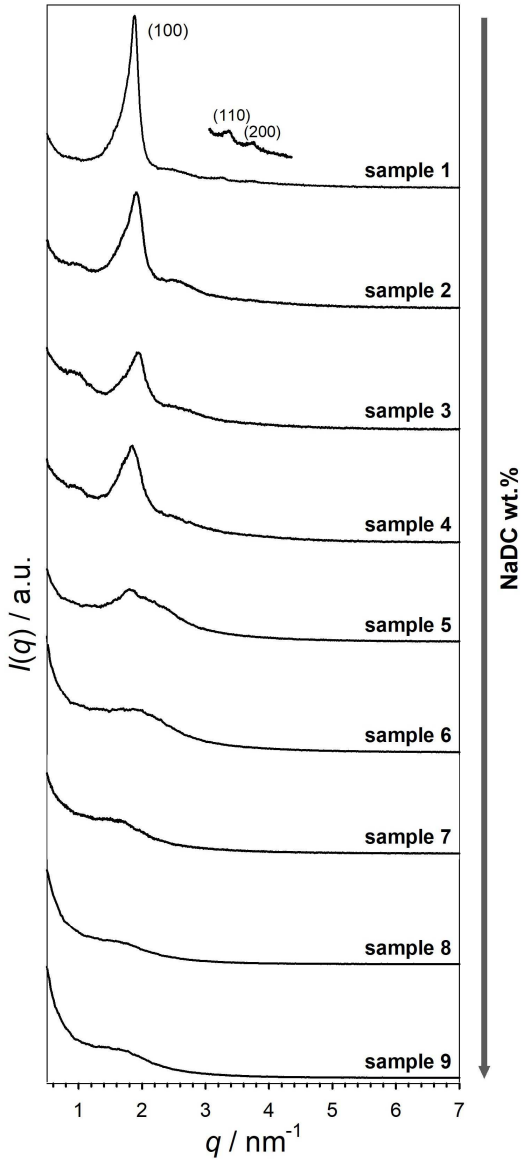

Fig. 4 SAXS patterns recorded on the different samples prepared upon increase of NaDC wt.%.

From all the reported analysis it is clear that the introduction of the NaDC induces the change in morphology and the variation of the sole concentration of NaDC allows tuning of the particle shape. The modulation determined by NaDC is initially gradual but becomes dramatic when more than 30 wt.% of NaDC is employed. This is also reflected in the gradual loss of mesostructure ordering revealed by SAXS patterns.

In our previous work[40] we proposed that the remarkable effect of bile salts is due to a variation of interactions at the interface between CTA^+ micelles and silicate polyanions. It is known that the bile salt intercalates into the micelle core and stabilizes the aggregate through

attractive electrostatic interactions between the carboxylate groups and the charged CTA^+ groups, subsequently inducing a variation of the micelle charge density.[48] The screening of positive charges would cause a delay in silicates adsorption and condensation, leading to a non-isotropic growth of particles. In addition, the decrease of surface charge density would induce a lowering of the micelle curvature, with formation of elongated micelles, at higher concentration of bile salt.

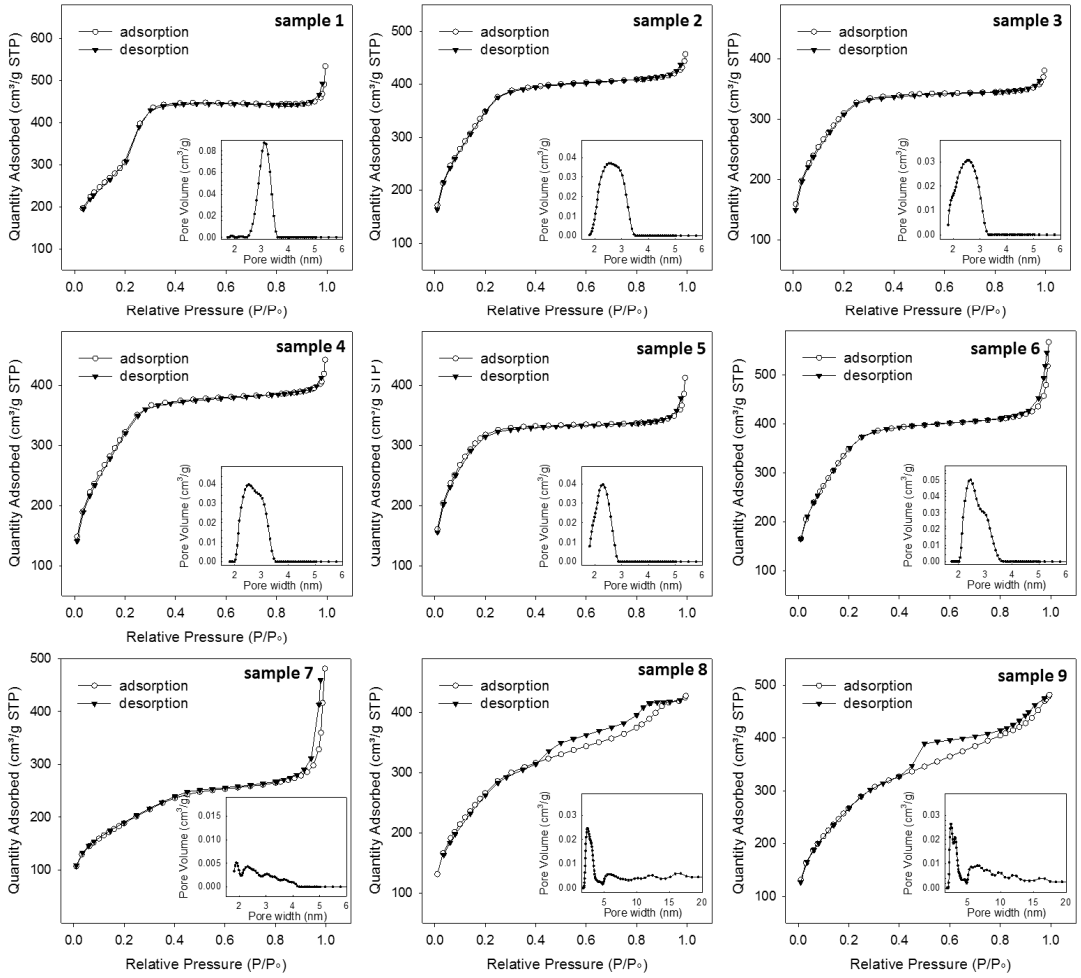

Fig. 5 Nitrogen adsorption/desorption isotherms of samples prepared with increasing amounts of NaDC. Related pore width distributions are reported in the insets.

Table 2 Porosity properties of the particles. a) Calculated from unit cell a_0 as defined in paragraph 2.3, b) calculated from the adsorption branch according to density functional theory (DFT) method assuming the cylindrical geometry. The value corresponding to the maximum of the distribution is reported.

Sample	Average pore diameter[a] (SAXS) (nm)*	Average pore diameter (N_2 ads)[b] (nm)	Total pore volume (cm^3/g)	BET specific area (m^2/g)
1	2.9	2.9	0.61	1294
2	2.7	2.7	0.60	1248
3	-	2.6	0.51	1063
4	-	2.5	0.57	1189
5	-	2.3	0.48	1042
6	-	2.4	0.69	1228
7	-	2-4	0.31	671
8	-	3.0	0.62	961
9	-	3.0	0.65	984

***Estimation of the average pore diameter from SAXS analysis was performed only for those cases in which the presence of long-range order permitted to extrapolate reliable data from calculations.

The hypothesis of a non-isotropic growth is supported by the gradual flattening of the particles accompanied by increase of their width and it leads to the formation of hexagonal platelets, if compared to the spherical particles formed in the presence of only CTAB. However, once NaDC concentration has been further increased the insertion of the steroidal backbone between CTAB molecules would induce a significant lowering of the micelle curvature and subsequent growth of the micelle in length.[48] This would lead to the formation of elongated composite structures such as the rods present in sample 4 (NaDC 15 wt.%) and this hypothesis may also explain the pore diameter values observed upon increase of NaDC wt.%. According to Israelachvili's geometry rules,[59] commonly used to predict aggregation behaviors of conventional surfactants, the insertion of NaDC into the micelles core would in fact increase the average volume per surfactant molecule and decrease the critical length, resulting in a decrease of the micelle diameter and, subsequently, of the pore width. The insertion of an increasing number of molecules has as consequences the gradual loss of long-range order in the structure, clearly shown by the evolution of SAXS patterns (Fig. 4), and the appearance of a curvature of the particles, with the formation of curved rods

(samples 5 and 6) and of toroidal structures (sample 7). In fact, the insertion of the bile salt into the micelles implies a decrease of their surface charge, thus weakening their reciprocal long-range interaction and inhibiting the formation of ordered mesostructures. Reasonably, in these conditions the elongated mixed micelles may associate into flexible bundles, thus templating the formation of curved particles. Interestingly, in sample 5 (NaDC 30 wt.%) several different morphologies could be imaged. Such observation could be linked to a critical concentration of NaDC vs CTAB that is high enough to induce the formation of elongated materials but still it is not enough to yield mainly curved rods, and then toroidal particles. The latter ones most probably form in order to reduce the surface energy at the extremes of fibers growing in length upon further NaDC addition. As mentioned before, samples 6-7 did not withstand the calcination process, most probably due to the collapse of the walls of the long pore channels. The formation of hetereogenous and disordered materials in samples 8 and 9 can be instead due to a significant variation of micelles charge that affects the interactions with the silicate, leading to weaker interactions and to less organized materials. This would also be in agreement with the above mentioned lower amount of MSPs recovered for these two samples. In fact, for these mixture compositions, the decrease of micellar charge density may be so pronounced to induce weaker interactions with the silicates and therefore production of smaller amounts of material.

The results clearly suggest that the evolution of the mixed micellar templates at different surfactant ratios determines the particle morphology variation, since the magnitude of interactions between the templating micelles and the silicates species varies. To have a full understanding of the template role in the formation of the different morphologies, we investigated the CTAB/NaDC mixed micelles at the surfactant ratios used for the particles preparation and we studied the evolution of the micelle size by means of dynamic light scattering (DLS) and that of the superficial charge through electrophoretic mobility (μ) determination. We analyzed samples containing CTAB 20.0 mM in Milli-Q water and an increasing amount of NaDC (2.5 to 90 wt.% vs. CTAB). The measurements were performed at concentrations higher than those employed in the MSPs preparation (CTAB 5.5 mM) in order to have a significant scattering and reduced noise. Nevertheless, it can be reasonably assumed that the different concentration does not induce a variation in size and shape of the aggregates since CTAB is reported to form spherical micelles both at 20.0 and 5.5 mM.[60] Moreover, we can exclude a contribution of free NaDC micelles which could be

concentration-dependent, due to the strong electrostatic driving force in the formation of mixed aggregates.

The apparent hydrodynamic diameters (D_h), the μ values and the normalized average intensity were reported in Fig. 6. The electrophoretic mobility data showed that the progressive addition of NaDC to CTAB determined a gradual lowering of the charge of the aggregates, thus confirming the inclusion of NaDC in the micelles and the neutralization of the CTA^+ charge. Concerning the hydrodynamic diameters, starting from the lowest NaDC wt.% an increase of the NaDC fraction dictated no significant variations up to NaDC 30 wt.% By contrast, a remarkable increase of the size of the mixed micelles was observed at higher NaDC fractions. The observed trend was reproduced by the normalized average intensity. Both the D_h and the intensity data suggest that NaDC 30 wt.% represents a critical composition for the co-assembly of the oppositely charged surfactant in the mixture, as it marks the starting point for a significant NaDC-induced growth of worm-like mixed micelles. In addition, DLS and synchrotron-SAXS characterization on the same samples after three weeks from preparation suggested that in the surfactant mixtures larger aggregates with D_h values of 10-20 nm and about 100 nm could grow at room temperature (Fig. S11). The growth occurred in the range 2.5-50 NaDC wt.% and gave rise to a maximum of both light scattering and synchrotron-SAXS intensity at 30 wt%. No significant variation of the DLS data with aging was observed at large NaDC fractions (70-90 wt.%). The synchrotron-SAXS data in the higher q range, mainly related to the smaller species, suggested that rod- or worm-like mixed aggregates with a core-shell electron density typical of CTAB micelles were present in the solution and showed a decreasing trend of the core radius and shell thickness with increasing NaDC content (Fig. S12). These effects could be ascribed to both a release of the Br^- counterions from the aggregate surface[61] and the intercalation of the NaDC molecules, with consequent increase of the average packing parameter per surfactant molecule as noted before. The decrease in core radius was particularly evident for the samples with 70 and 90 wt.% NaDC content and could be correlated with the observation of small porosity and low amount of material obtained in the synthetic procedure for samples 8 and 9.

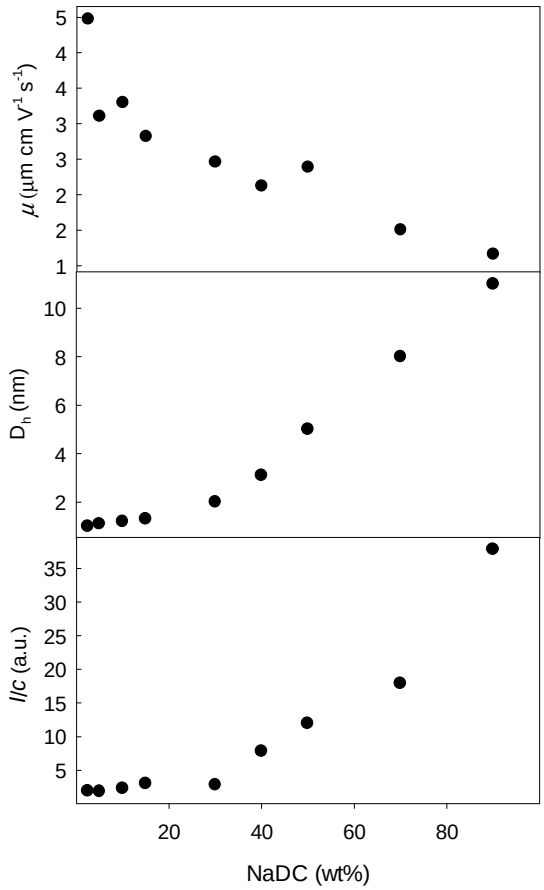

Fig. 6. Electrophoretic mobility (μ), hydrodynamic diameter (D_h) and reduced intensity (I/c) as a function of NaDC wt% for micelles in the CTAB/NaDC mixtures at 25 °C.

Although the silica condensation process adds significant complexity to the system,[62] these results could elucidate the behavior of the CTAB/NaDC mixtures in the preparation of the silica particles. In particular, they would show that small highly charged micelles are formed at low NaDC fraction were flat silica particles are formed, whereas elongated worm-like micelles are formed at higher NaDC content where rod-like particles are obtained. The rods would progressively curve and close into toroids in parallel with a NaDC-induced progressive growth of micelles. Interestingly, a borderline composition could be identified at NaDC 30 wt.%, in between those providing globular micelles and elongated worm-like ones where, accordingly, a mixture of flat and elongated silica particles was obtained. To better visualize the correlation between the mixed micelles evolution and the effect on the particle growth, a schematic representation is depicted in Scheme 1.

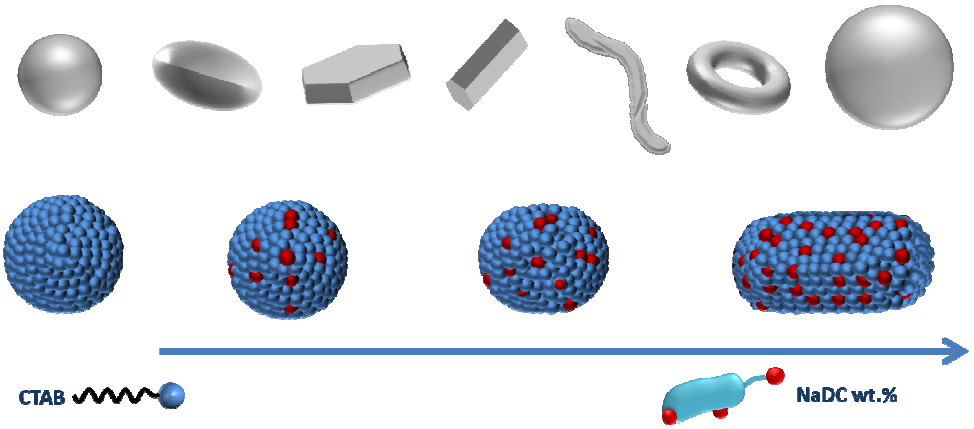

Scheme 1 Schematic representation of the evolution of the CTAB/NaDC mixed micelles and the related variation of particle shape.

5. Conclusions

In the attempt to develop simple, room temperature, synthetic methodologies to control the morphology of mesoporous silica nanoparticles we have investigated the effect of different compositions of CTAB/NaDC mixtures, which act as templates for the mesoporous silica formation. Tuning of the particle shape was achieved by varying the sole NaDC concentration in alkaline aqueous media. Flat particles formed at low concentrations of NaDC, whereas the growth of elongated particles was induced when the bile salt concentration was increased. The morphology modulation is explained by the specific interactions between the two counter-charged surfactants and by the variation of the properties of the templating mixed micelles. CTAB/NaDC mixtures are promising templating systems to be used for controlling the morphology of mesoporous silica particles.

Notes

The authors declare no competing financial interest.

Acknowledgements

This work was financially supported by the European Union through the SACS Project (grant N° 310651). L.D.C. gratefully acknowledges AXA Research funds for financial support. Parts of this research was carried out at SWING beamline at SOLEIL (proposal

21071241) and supported by the project CALIPSOplus under the Grant Agreement 730872 from the EU Framework Programme for Research and Innovation HORIZON 2020. We thank J. Perez for assistance during the experiments.

References

[1] I.I. Slowing, B.G. Trewyn, S. Giri, V.S.Y. Lin, Mesoporous Silica Nanoparticles for Drug Delivery and Biosensing Applications, Adv. Funct. Mater., 17 (2007) 1225-1236.
[2] Z. Li, J.C. Barnes, A. Bosoy, J.F. Stoddart, J.I. Zink, Mesoporous silica nanoparticles in biomedical applications, Chem. Soc. Rev. 41 (2012) 2590-2605.
[3] I.I. Slowing, J.L. Vivero-Escoto, B.G. Trewyn, V.S.Y. Lin, Mesoporous silica nanoparticles: structural design and applications, J. Mater. Chem., 20 (2010) 7924-7937.
[4] Y. Wan, Zhao, On the Controllable Soft-Templating Approach to Mesoporous Silicates, Chem. Rev., 107 (2007) 2821-2860.
[5] S.-H. Wu, C.-Y. Mou, H.-P. Lin, Synthesis of mesoporous silica nanoparticles, Chem. Soc. Rev., 42 (2013) 3862-3875.
[6] D. Tarn, C.E. Ashley, M. Xue, E.C. Carnes, J.I. Zink, C.J. Brinker, Mesoporous Silica Nanoparticle Nanocarriers: Biofunctionality and Biocompatibility, Acc. Chem. Res., 46 (2013) 792-801.
[7] X. Du, X. Li, L. Xiong, X. Zhang, F. Kleitz, S.Z. Qiao, Mesoporous silica nanoparticles with organo-bridged silsesquioxane framework as innovative platforms for bioimaging and therapeutic agent delivery, Biomaterials, 91 (2016) 90-127.
[8] J.G. Croissant, Y. Fatieiev, A. Almalik, N.M. Khashab, Mesoporous Silica and Organosilica Nanoparticles: Physical Chemistry, Biosafety, Delivery Strategies, and Biomedical Applications, Adv. Healthcare Mater., 7 (2018) 1700831.
[9] L. Travaglini, P. Picchetti, R. Totovao, E, A. Prasetyanto, L. De Cola, Highly degradable imine-doped mesoporous silica particles, Mater. Chem. Front., 3 (2019) 111-119.
[10] H.-Y. Chiu, D. Gößl, L. Haddick, H. Engelke, T. Bein, Clickable Multifunctional Large-Pore Mesoporous Silica Nanoparticles as Nanocarriers, Chem. Mater., 30 (2018) 644-654.
[11] C. Argyo, V. Weiss, C. Bräuchle, T. Bein, Multifunctional Mesoporous Silica Nanoparticles as a Universal Platform for Drug Delivery, Chem. Mater., 26 (2014) 435-451.
[12] M. Manzano, V. Aina, C.O. Areán, F. Balas, V. Cauda, M. Colilla, M.R. Delgado, M. Vallet-Regí, Studies on MCM-41 mesoporous silica for drug delivery: Effect of particle morphology and amine functionalization, Chem. Eng. J., 137 (2008) 30-37.
[13] X. Huang, X. Teng, D. Chen, F. Tang, J. He, The effect of the shape of mesoporous silica nanoparticles on cellular uptake and cell function, Biomaterials, 31 (2010) 438-448.
[14] X. Huang, L. Li, T. Liu, N. Hao, H. Liu, D. Chen, F. Tang, The Shape Effect of Mesoporous Silica Nanoparticles on Biodistribution, Clearance, and Biocompatibility in Vivo, ACS Nano, 5 (2011) 5390-5399.
[15] N. Hao, L. Li, F. Tang, Shape matters when engineering mesoporous silica-based nanomedicines, Biomater. Sci., 4 (2016) 575-591.
[16] K.J. Edler, Current Understanding of Formation Mechanisms in Surfactant-Templated Materials, Aust. J. Chem., 58 (2005) 627-643.
[17] K. Holmberg, Surfactant-templated nanomaterials synthesis, J. Colloid Interface Sci., 274 (2004) 355-364.
[18] C. Yu, J. Fan, B. Tian, D. Zhao, Morphology Development of Mesoporous Materials: a Colloidal Phase Separation Mechanism, Chem. Mater., 16 (2004) 889-898.
[19] H.B.S. Chan, P.M. Budd, T.d. Naylor, Control of mesostructured silica particle morphology, J. Mater. Chem., 11 (2001) 951-957.

[20] Q. Qu, G. Zhou, Y. Ding, S. Feng, Z. Gu, Adjustment of the morphology of MCM-41 silica in basic solution, J. Non-Cryst. Solids, 405 (2014) 104-115.
[21] H.-P. Lin, C.-Y. Mou, Structural and Morphological Control of Cationic Surfactant-Templated Mesoporous Silica, Acc. Chem. Res., 35 (2002) 927-935.
[22] H. Yang, G. Vovk, N. Coombs, I. Sokolov, G. A. Ozin, Synthesis of mesoporous silica spheres under quiescent aqueous acidic conditions, J. Mater. Chem., 8 (1998) 743-750.
[23] S.P. Naik, S.P. Elangovan, T. Okubo, I. Sokolov, Morphology Control of Mesoporous Silica Particles, J. Phys. Chem. C, 111 (2007) 11168-11173.
[24] E.M. Björk, F. Söderlind, M. Odén, Tuning the Shape of Mesoporous Silica Particles by Alterations in Parameter Space: From Rods to Platelets, Langmuir, 29 (2013) 13551-13561.
[25] P. Linton, H. Wennerstrom, V. Alfredsson, Controlling particle morphology and size in the synthesis of mesoporous SBA-15 materials, PCCP, 12 (2010) 3852-3858.
[26] L. Han, Y. Zhou, T. He, G. Song, F. Wu, F. Jiang, J. Hu, One-pot morphology-controlled synthesis of various shaped mesoporous silica nanoparticles, J. Mater. Sci., 48 (2013) 5718-5726.
[27] M. Grün, K.K. Unger, A. Matsumoto, K. Tsutsumi, Novel pathways for the preparation of mesoporous MCM-41 materials: control of porosity and morphology, Microporous Mesoporous Mater., 27 (1999) 207-216.
[28] B. Wang, C. Chi, W. Shan, Y. Zhang, N. Ren, W. Yang, Y. Tang, Chiral Mesostructured Silica Nanofibers of MCM-41, Angew. Chem. Int. Ed., 45 (2006) 2088-2090.
[29] Q. Cai, Z.-S. Luo, W.-Q. Pang, Y.-W. Fan, X.-H. Chen, F.-Z. Cui, Dilute Solution Routes to Various Controllable Morphologies of MCM-41 Silica with a Basic Medium, Chem. Mater., 13 (2001) 258-263.
[30] N. Hao, X. Chen, K.W. Jayawardana, B. Wu, M. Sundhoro, M. Yan, Shape control of mesoporous silica nanomaterials templated with dual cationic surfactants and their antibacterial activities, Biomater. Sci., 4 (2016) 87-91.
[31] X. Wang, Y. Zhang, W. Luo, A.A. Elzatahry, X. Cheng, A. Alghamdi, A.M. Abdullah, Y. Deng, D. Zhao, Synthesis of Ordered Mesoporous Silica with Tunable Morphologies and Pore Sizes via a Nonpolar Solvent-Assisted Stöber Method, Chem. Mater., 28 (2016) 2356-2362.
[32] H. Yang, N. Coombs, G.A. Ozin, Morphogenesis of shapes and surface patterns in mesoporous silica, Nature, 386 (1997) 692.
[33] V. Giglio, S. Varela-Aramburu, L. Travaglini, F. Fiorini, P.H. Seeberger, L. Maggini, L. De Cola, Reshaping Silica Particles: Mesoporous Nanodiscs for Bimodal Delivery and Improved Cellular Uptake, Chem. Eng. J., 340 (2018) 148-154.
[34] J. Croissant, X. Cattoën, M.W.C. Man, P. Dieudonné, C. Charnay, L. Raehm, J.O. Durand, One-Pot Construction of Multipodal Hybrid Periodic Mesoporous Organosilica Nanoparticles with Crystal-Like Architectures, Adv. Mater., 27 (2015) 145-149.
[35] J.G. Croissant, Y. Fatieiev, H. Omar, D.H. Anjum, A. Gurinov, J. Lu, F. Tamanoi, J.I. Zink, N.M. Khashab, Periodic Mesoporous Organosilica Nanoparticles with Controlled Morphologies and High Drug/Dye Loadings for Multicargo Delivery in Cancer Cells, Chem. Eur. J., 22 (2016) 9607-9615.
[36] A. Sayari, S. Hamoudi, Y. Yang, I.L. Moudrakovski, J.R. Ripmeester, New Insights into the Synthesis, Morphology, and Growth of Periodic Mesoporous Organosilicas, Chem. Mater., 12 (2000) 3857-3863.
[37] S. Sadasivan, D. Khushalani, S. Mann, Synthesis and shape modification of organo-functionalised silica nanoparticles with ordered mesostructured interiors, J. Mater. Chem., 13 (2003) 1023-1029.
[38] X. Du, J. He, Elaborate control over the morphology and structure of mercapto-functionalized mesoporous silicas as multipurpose carriers, Dalton Trans., 39 (2010) 9063-9072.
[39] S. Huh, J.W. Wiench, J.-C. Yoo, M. Pruski, V.S.Y. Lin, Organic Functionalization and Morphology Control of Mesoporous Silicas via a Co-Condensation Synthesis Method, Chem. Mater., 15 (2003) 4247-4256.
[40] L. Travaglini, L. De Cola, Morphology Control of Mesoporous Silica Particles Using Bile Acids as Cosurfactants, Chem. Mater., 30 (2018) 4168-4175.

[41] D. Madenci, S.U. Egelhaaf, Self-assembly in aqueous bile salt solutions, Curr. Opin. Colloid Inter. Sci., 15 (2010) 109-115.
[42] L. Galantini, M.C. di Gregorio, M. Gubitosi, L. Travaglini, J.V. Tato, A. Jover, F. Meijide, V.H. Soto Tellini, N.V. Pavel, Bile salts and derivatives: Rigid unconventional amphiphiles as dispersants, carriers and superstructure building blocks, Curr. Opin. Colloid Inter. Sci., 20 (2015) 170-182.
[43] A. Bonincontro, G. Briganti, A.A. D'Archivio, L. Galantini, E. Giglio, Structural Study of the Micellar Aggregates of Sodium Taurodeoxycholate, J. Phys. Chem. B, 101 (1997) 10303-10309.
[44] A. Bonincontro, A. A. D'Archivi, L. Galantini, E. Giglio, F. Punzo, On the Micellar Aggregates of Alkali Metal Salts of Deoxycholic Acid, J. Phys. Chem. B, 103 (1999) 4986-4991.
[45] M. C. di Gregorio, L. Travaglini, A. Del Giudice, J. Cautela, N. V. Pavel, L. Galantini, Bile Salts: Natural Surfactants and Precursors of a Broad Family of Complex Amphiphiles, Langmuir, DOI: 10.1021/acs.langmuir.8b02657
[46] M. Swanson-Vethamuthu, M. Almgren, P. Hansson, J. Zhao, Surface Tension Studies of Cetyltrimethylammonium Bromide−Bile Salt Association, Langmuir, 12 (1996) 2186-2189.
[47] P.K. Jana, S.P. Moulik, Interaction of bile salts with hexadecyltrimethylammonium bromide and sodium dodecyl sulfate, J. Phys. Chem., 95 (1991) 9525-9532.
[48] M. Swanson-Vethamuthu, M. Almgren, G. Karlsson, P. Bahadur, Effect of Sodium Chloride and Varied Alkyl Chain Length on Aqueous Cationic Surfactant−Bile Salt Systems. Cryo-TEM and Fluorescence Quenching Studies, Langmuir, 12 (1996) 2173-2185.
[49] C. La Mesa, A. Khan, K. Fontell, B. Lindman, Phase diagrams and NMR studies of some ternary sodium deoxycholate-surfactant-water systems, J. Colloid Interface Sci., 103 (1985) 373-391.
[50] M.E. Haque, A.R. Das, A.K. Rakshit, S.P. Moulik, Properties of Mixed Micelles of Binary Surfactant Combinations, Langmuir, 12 (1996) 4084-4089.
[51] M.S. Vethamuthu, M. Almgren, E. Mukhtar, P. Bahadur, Fluorescence quenching studies of the aggregation behavior of the mixed micelles of bile salts and cetyltrimethylammonium halides, Langmuir, 8 (1992) 2396-2404.
[52] L. Jiang, K. Wang, M. Deng, Y. Wang, J. Huang, Bile Salt-Induced Vesicle-to-Micelle Transition in Catanionic Surfactant Systems: Steric and Electrostatic Interactions, Langmuir, 24 (2008) 4600-4606.
[53] C. Liu, J. Cui, A. Song, J. Hao, A bile acid-induced aggregation transition and rheological properties in its mixtures with alkyltrimethylammonium hydroxide, Soft Matter, 7 (2011) 8952-8960.
[54] C.M.C. Faustino, C.S. Serafim, I.N. Ferreira, M.A. Branco, A.R.T. Calado, L. Garcia-Rio, Mixed Micelle Formation between an Amino Acid-Based Anionic Gemini Surfactant and Bile Salts, Ind. Eng. Chem. Res., 53 (2014) 10112-10118.
[55] S. Chavda, D. Danino, V.K. Aswal, K. Singh, D.G. Marangoni, P. Bahadur, Microstructure and transitions in mixed micelles of cetyltrimethylammonium tosylate and bile salts, Colloids Surf. A, 513 (2017) 223-233.
[56] S. Brunauer, P.H. Emmett, E. Teller, Adsorption of Gases in Multimolecular Layers, J. Am. Chem. Soc., 60 (1938) 309-319.
[57] M. Jaroniec, M. Kruk, J. P. Olivier, S. Koch, A new method for the accurate pore size analysis of MCM-41 and other silica based mesoporous materials, Stud. Surf. Sci. Cat., 128 (2000) 71-80.
[58] C.-Y. Chen, H.-X. Li, M.E. Davis, Studies on mesoporous materials: I. Synthesis and characterization of MCM-41, Microporous Materials, 2 (1993) 17-26.
[59] J.N. Israelachvili, D.J. Mitchell, B.W. Ninham, Theory of self-assembly of hydrocarbon amphiphiles into micelles and bilayers, J. Chem. Soc., Faraday Trans.2, 72 (1976) 1525-1568.
[60] Z. Lin, J.J. Cai, L.E. Scriven, H.T. Davis, Spherical-to-Wormlike Micelle Transition in CTAB Solutions, J. Phys. Chem., 98 (1994) 5984-5993.
[61] V. Lutz-Bueno, M. Liebi, J. Kohlbrecher, P. Fischer, Intermicellar Interactions and the Viscoelasticity of Surfactant Solutions: Complementary Use of SANS and SAXS, *Langmuir*, 33 (2017) 2617-2627.
[62] F. Michaux, N. Baccile, M. Impéror-Clerc, L. Malfatti, N. Folliet, C. Gervais, S. Manet, F. Meneau, J.S. Pedersen, F. Babonneau, In Situ Time-Resolved SAXS Study of the Formation of Mesostructured

Organically Modified Silica through Modeling of Micelles Evolution during Surfactant-Templated Self-Assembly, Langmuir, 28 (2012) 17477-17493.

Graphical Abstract